the design method of the blood pump has not been established yet because the type number of the blood pump is generally low and the internal flow tend to be complex, and moreover the conditions of the occurrence of the hemolysis and the thrombosis are not clear quantitatively as the characteristics of the blood are individually different. Therefore, based on the design method for general industrial centrifugal pumps [4], the authors designed a two-stage centrifugal blood pump (Prototype 1) in the previous study [1], using the knowledge for the suppression of the hemolysis and the thrombosis in single stage blood pumps. The flow rate, the pump head, and the rotational speed at the design point are 3L/min, 500mmHg, and 4200rpm, respectively. The cross-sections of Prototype 1 are shown in Fig.4. The geometry of the pump is briefly explained in the present paper as the details have been commented in the reference [1]. The cross-sections from A to F in Fig.4 are shown in Fig.5. The working fluid flows into the pump through the suction volute shown in Fig.5(a), passes through the 1st impeller (Fig.5(c)), the return channel (Fig.5(d)), the 2nd impeller (Fig.5(f)), and flows out from the pump through the double volute (Fig.5(f)). The black dots in Fig.5 shows the measuring points of pressures and their names are shown in the sides of them.

The specifications of Prototype 1 are shown in Table 1. Prototype 1 has semi-open impellers and the diameters D_t of them are

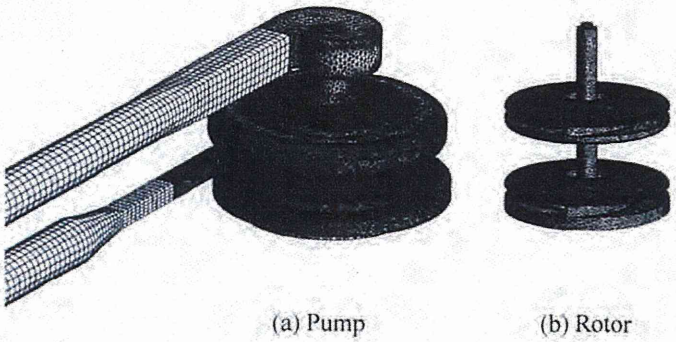

(a) Pump (b) Rotor

Fig. 3 Computational grid on the wall surface of Prototype 2

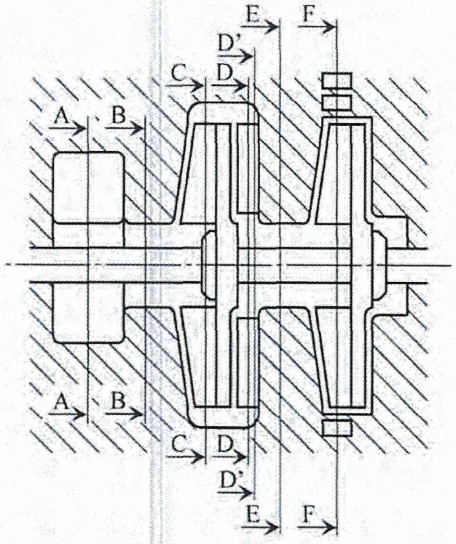

Fig. 4 Meridian cross-section of Prototype 1

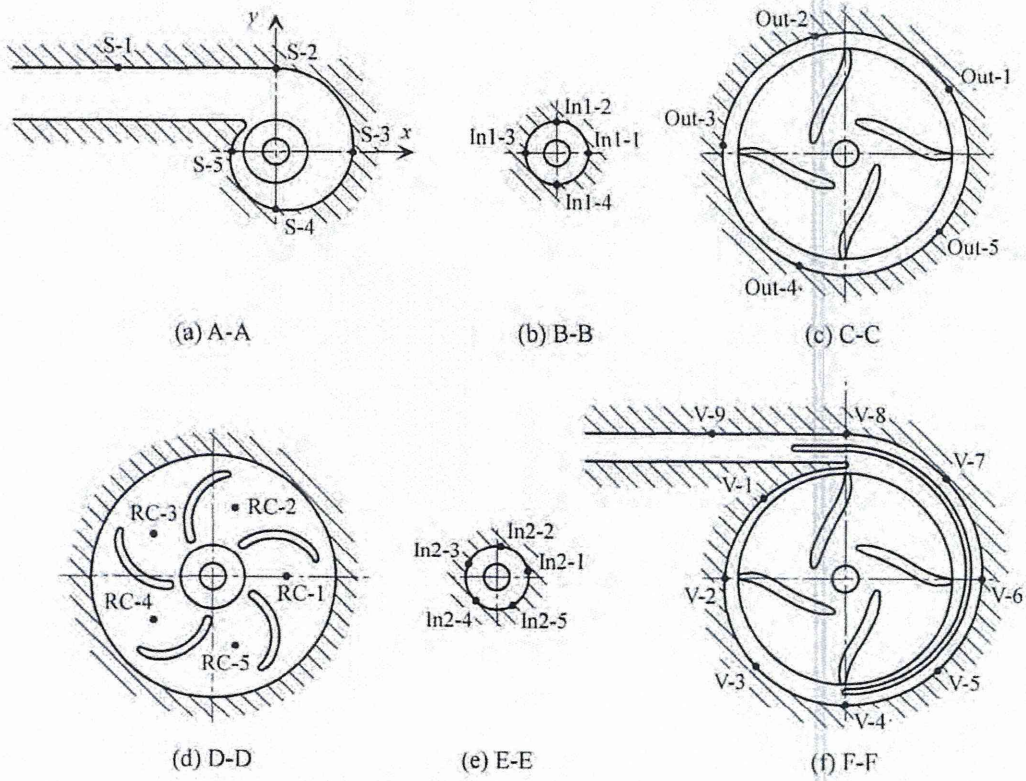

(a) A-A (b) B-B (c) C-C

(d) D-D (e) E-E (f) F-F

Fig. 5 Cross-section of Prototype 1 and the position of holes for the measurement of pressure distribution

as small as 40mm. The priming volume of the pump are also as small as 42ml in consideration of the application for pediatric patients. The shape of the blades of 1st and 2nd impellers are the same and two-dimensional. The inlet and outlet blade angles of the impeller, β_1 and β_2, are 4.7deg and 80deg, respectively. The number of the blades is 4 and the tip clearance is 1mm. The return channel shown in Fig.5(d) has 5 return guide vanes whose blade angles at the inlet and the outlet are 2deg and 90deg, respectively.

As the demanded pump performance of 500mmHg at 3L/min was achieved at the rotational speed of 4000rpm in the experiment, 4000rpm was chosen as the reference rotational speed in the present study.

4.2 Anti-Hemolysis and Thrombosis Performances

Kameneva et al. [5] examined the blood flow in a narrow tube with the inner diameter of 1mm and showed that the amount of the hemolysis drastically increased when the shear stress on the blood was larger than 200Pa. Therefore, the shear stress of 200Pa was used as a threshold of the hemolysis in the present study. The wall shear stress in Prototype 1 is shown in Fig.6. In the operation of 1150rpm with the water, the threshold of the shear stress for the hemolysis is about 16Pa, based on the similarity law of $\tau_{water} = \tau_{blood} \cdot \rho_{water} \cdot U_{t,water}^2 / (\rho_{blood} \cdot U_{t,blood}^2)$. The shear stress larger than 16Pa is observed on the casing wall near the tip of the 1st and 2nd impellers (Figs.6(a) and (d)), the periphery of the backshroud of the 1st impeller (Fig.6(b)), and the tongue of the double volute casing (Fig.6(e)). For the suppression of the hemolysis, it was found that the reduction of these high shear stresses was needed.

Figure 7 shows the velocity vector on the cross-section D'-D' in Fig.4, which is in the return channel and 0.5mm away from the casing wall. As shown in Fig.7, the flow separates from the blade and the stagnation occurs in the center of the vortex, which can cause the thrombosis. Therefore, it was found that the improvement of the return guide vane was necessary for the suppression of the thrombosis.

Table 1 Specification of Prototype 1

Type of impeller	Semi-open
Number of blade	4
Diameter of impeller, D_t [mm]	40
Inlet blade angle, β_1 [deg]	4.7
Outlet blade angle, β_2 [deg]	80.0
Blade height at the inlet, h_1[mm]	5.0
Blade height at the outlet, h_2[mm]	3.0
Tip clearance, C [mm]	1.0
Design flow rate [L/min]	3.0
Design pump head [mmHg]	500

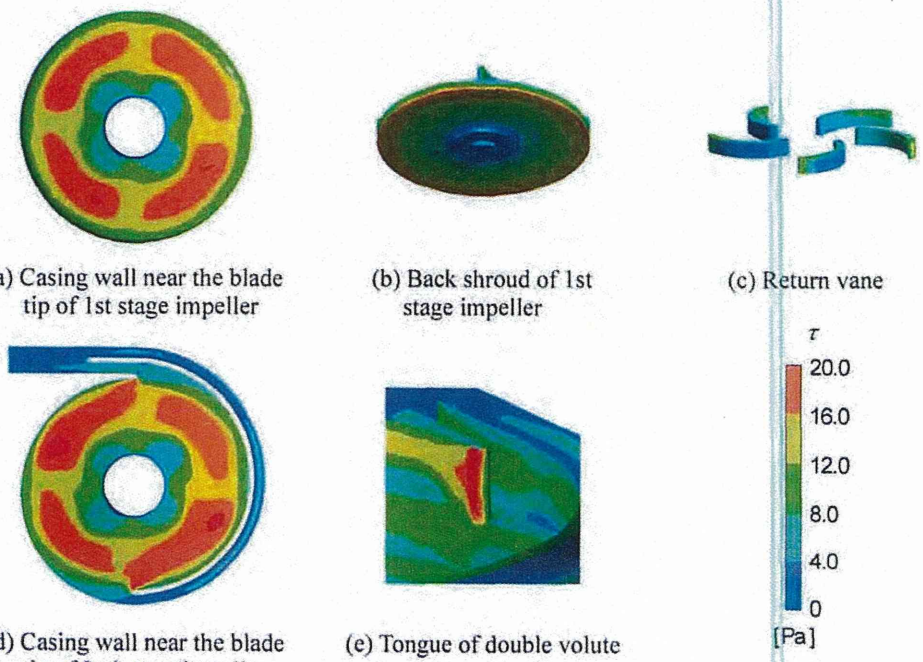

(a) Casing wall near the blade tip of 1st stage impeller

(b) Back shroud of 1st stage impeller

(c) Return vane

(d) Casing wall near the blade tip of 2nd stage impeller

(e) Tongue of double volute

Fig. 6 Wall shear stress distribution on Prototype 1 at $Q=Q_d$, N=1150 rpm [1]

Improvement of the Pump and Hemolysis Test

5.1 Geometry of the Improved Pump (Prototype 2)

Prototype 1 has problems with regard to the anti-hemolysis and thrombosis performances, which were described in 4.2. To solve these problems, a pump was newly designed. The cross-sections of the new pump (Prototype 2) are shown in Fig.8. With a view to a practical use of Prototype 2, pivot bearings are adopted and the impellers are driven by attractive forces of neodymium magnets in the backshroud of the 2nd impeller and a driving rotor outside the pump. The cross-sections from A to F in Fig.8 are

Fig. 7 Velocity vector on the cross-section (D'-D' in Fig.4) of the return channel in Prototype 1 at $Q=Q_d$. N=1150rpm. The distance of the cross-section D'-D' from the casing wall is 0.5mm [1]

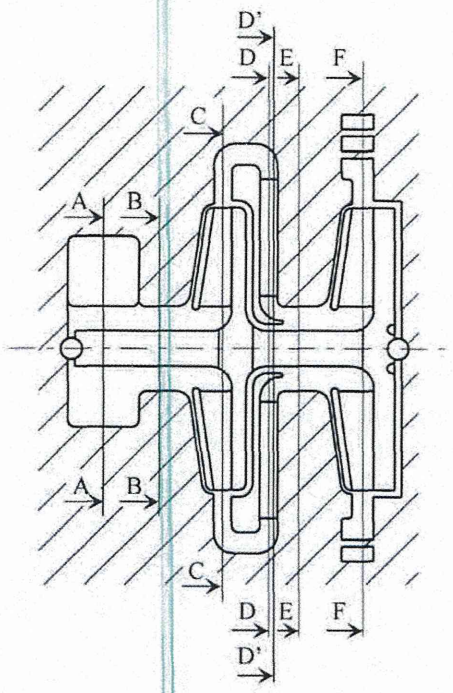

Fig. 8 Meridian cross-section of Prototype 2

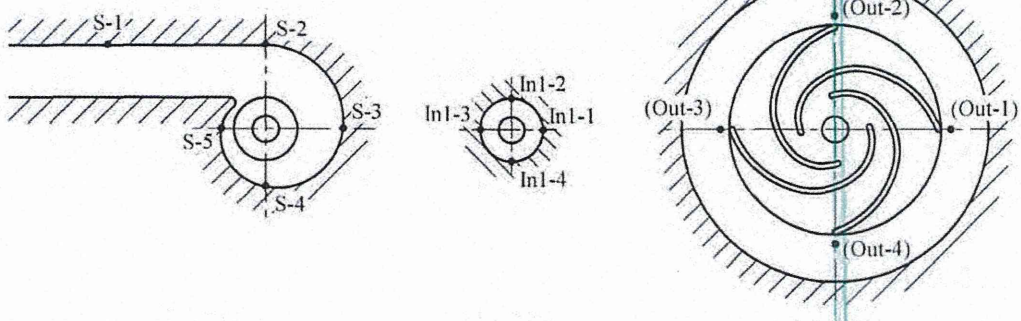

(a) A-A (b) B-B (c) C-C

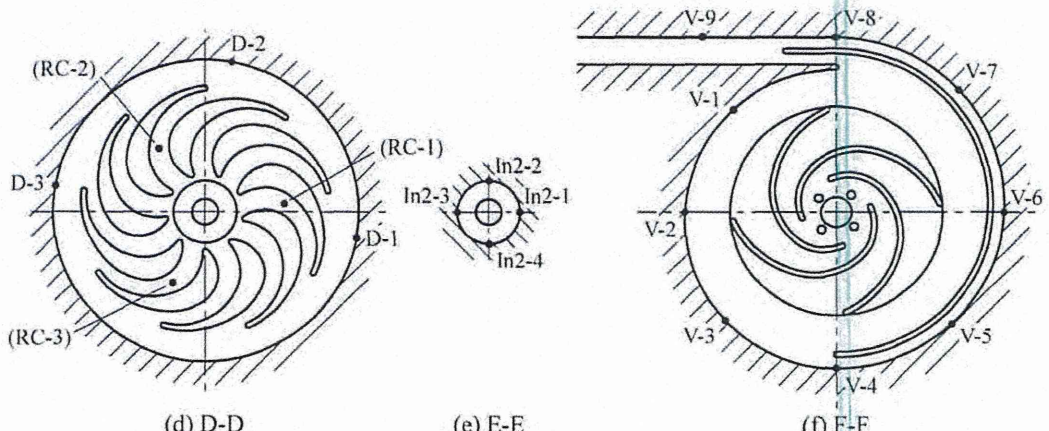

(d) D-D (e) E-E (f) F-F

Fig. 9 Cross-section of Prototype 2 and the position of holes for the measurement of pressure distribution

shown in Fig.9. As in Prototype 1, the working fluid flows into the pump through the suction volute shown in Fig.9(a), passes through the 1st impeller (Fig.9(c)), the return channel (Fig.9(d)), the 2nd impeller (Fig.9(f)), and flows out from the pump through the double volute (Fig.9(f)). The black dots in Fig.9 show the measuring points of pressure and their names are shown in the sides of them.

The specifications of Prototype 2 are shown in Table 2. Closed impellers were adopted because the front shroud of the impeller was effective for the decrease of the high shear stress on the casing wall near the tip of the impeller [1]. The clearance between the front shroud and the casing is 0.5mm. As a stagnation occurred in the impeller by applying the front shroud to the impellers of Prototype 1, the inlet and outlet blade angles have been changed into 15deg and 20deg, respectively. The process of the change of the blade angles is explained in detail in the next section. In Prototype 1, the flow velocity near the shaft in the clearance between the backshroud of the 2nd impeller and the casing was smaller and the thrombosis could occur there [1]. Therefore, four washout holes were made in the backshroud near the inlet of the 2nd impeller in Prototype 2. The washout holes increased the flow rate passing through the 2nd impeller and the flow stagnation was suppressed. For the suppression of the stagnation in the 1st impeller, the inlet and outlet blade heights, $h_{1,1st}$ and $h_{2,1st}$, were set to 4.5mm and 2.5mm, respectively, which are reduced by 0.5mm from those of the 2nd impeller. Besides, the design rotational speed was decreased from 4200rpm for Prototype 1 to 4000rpm for Prototype 2 because the pump head increased due to the attachment of the front shroud of the impellers.

In Prototype 1, the high shear stress occurred around the leading edge of the return guide vane and the tongue of the double volute casing, as shown in Figs.6(c) and (e). Based on the conservation law of the angular momentum, the circumferential velocity of the fluid which flows out from the impellers is smaller at larger radial positions. Therefore, the radial positions of the leading edge of the return guide vane and the tongue of the double volute casing were increased from 20mm to 24mm and from 21mm to 27mm, respectively. Owing to these modifications, the shear stress could be decreased sufficiently around the leading edge of the return guide vane and the tongue of the double volute casing, as we discuss later (Figs.13(c) and (e)). For the decrease of the high shear stress around the periphery of the 1st impeller, the shroud has been set to the return guide vane.

As shown in Fig.7, the stagnation which could cause the thrombosis occurred in the return channel of Prototype 1. For suppressing the stagnation, the larger blade thickness which covered the region of the flow separation was effective [1]. For giving an uniform radial flow at the outlet of the return channel, the larger number of blades were better [1]. Therefore, the geometry of the return guide vane was improved so that the vane covered the region of the flow separation and the number of the return guide vane was increased from 5 to 9. The return guide vane shown in Fig.9(d) was finally designed and could suppress the flow stagnation well, as we discuss later (Fig.14).

5.2 Installation of a Front Shroud on the Impeller and the Change of the Blade Angle

The instantaneous velocity vector in the impellers of Prototype 1 at $Q=Q_d$ is shown in Fig.10(a). The velocity vector on the plane which is 0.5mm away from the backshroud is shown and is a result at the time when the positional relation between the blade of the impeller and the casing is on the state shown in Fig.5. Figure 10(b) shows the results in the case that the front shroud was attached in the impeller of Prototype 1. In the case with the front shroud, the pump head increased by about 10% [1] and large vortices occurred, as shown in Fig.10(b). Especially, in the 1st impeller, as the vortices were stable and the stagnation was remarkable, the thrombosis was likely to occur. Therefore, to prevent the occurrence of the vortices, the outlet blade angles β_2 was changed into 15deg, 20deg, and 30deg in reference to β_2=22.5deg recommended by Stepanoff [6]. The blade shape was determined by the three-circular-arc method, as in the case of Prototype 1. The computations were conducted for these cases and the velocity vectors in the 1st impellers of β_2=15deg and 30deg were shown in Figs.11(a) and (b), respectively. In both cases, the impeller has the front shroud and the 2nd impeller has 4 washout holes. As shown in Fig.11(a), the fluid flows along the blade in the case of β_2=15deg. As shown in Fig.11(b), the flow separation occurs in the pressure side in the case of β_2=30deg which could generate the larger pump head. Finally, β_2 was set to 20deg. The velocity vectors in the case of β_2=20deg are shown in Fig.12. To realize the flow field and pump head similar to that in the 2nd impeller, the inlet and outlet blade heights, $h_{1,1st}$ and $h_{2,1st}$, of the 1st impeller were set to 4.5mm and 2.5mm, respectively, which were reduced by 0.5mm from those of the 2nd impeller. By the modification of the blade height, the flow fields in the 1st and 2nd impeller became similar and the large-scale stagnation due to the vortices could be suppressed, as shown in Fig.12. Although the decrease of β_2 causes the decrease of the pump head, the

Table 2 Specification of Prototype 2

Type of impeller	Closed
Number of blade	4
Diameter of impeller, D_t [mm]	40
Inlet blade angle, β_1 [deg]	15.0
Outlet blade angle, β_2 [deg]	20.0
Blade height of	
1st stage impeller at the inlet, $h_{1,1st}$ [mm]	4.5
1st stage impeller at the outlet, $h_{2,1st}$ [mm]	2.5
2nd stage impeller at the inlet, $h_{1,2nd}$ [mm]	5.0
2nd stage impeller at the outlet, $h_{2,2nd}$ [mm]	3.0
Clearance between front shroud and casing, C [mm]	0.5
Design flow rate [L/min]	3.0
Design pump head [mmHg]	500

demanded pump head was reserved by the modifications such as the attachment of the front shroud.

5.3 Anti-Hemolysis Performance

Figure 13 shows the wall shear stress of Prototype 2. The regions with the shear stress higher than 16Pa exist only on the casing wall near the inlet of the impellers, as shown in Figs.13(a) and (d). The area of the high wall shear stress in Prototype 2 is much smaller than the results shown in Fig.6 for Prototype 1. Therefore, it can be expected that Prototype 2 has a high anti-hemolysis performance.

5.4 Anti-Thrombosis Performance

Figure 14 shows the velocity vectors in the return channel of Prototype 2, which are the velocity vectors on the cross-section D'-D' shown in Fig.8. The stagnation does not appear in the return channel. Figure 15 shows the flow field in a meridian cross-section. The enlarged view of the clearance between the backshroud of the 1st impeller and the shroud of the return channel is shown in the left side of Fig.15. In the enlarged view, the fluid near the backshroud of the 1st impeller flows radially outward and the fluid near the shroud of the return channel flows radially inward. However, the velocity W/U_t in the clearance is as small as from about 0 to 0.1 and the possibility of the thrombosis cannot be denied. On the other hand, the velocity V/U_t in the clearance between the backshroud of the 2nd impeller and the casing is as large as from about 0.1 to 0.5. There is a part which is better to be

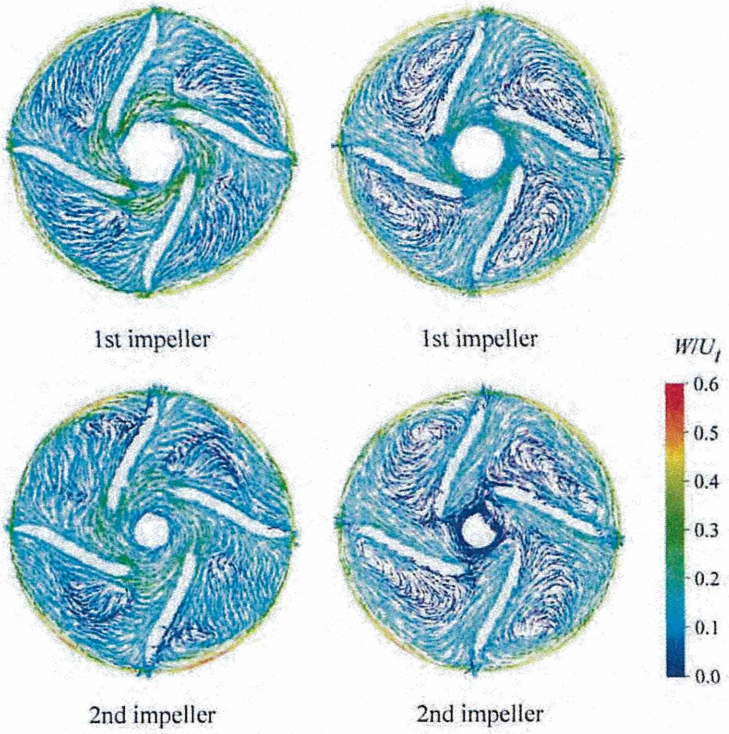

(a) Original (Prototype1) (b) Impeller with front shroud

Fig. 10 Velocity vector near the back shroud in the original and modified impellers of Prototype 1 at $Q=Q_d$

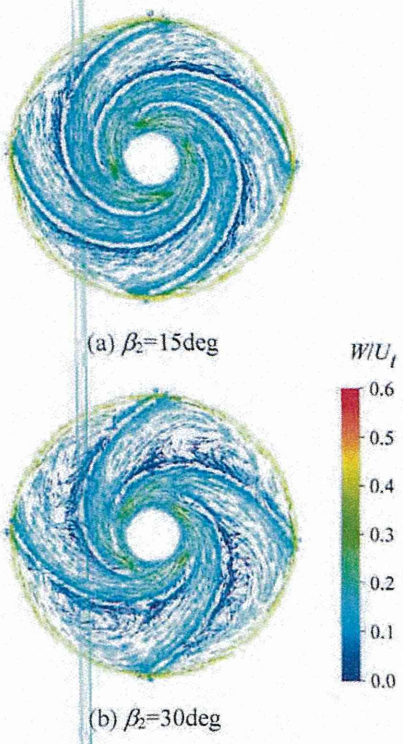

Fig. 11 Velocity vector near the back shroud of 1st impellers with β_2=15deg and 30deg. The impellers have front shroud and the 2nd impeller has four washout holes. $Q=Q_d$ and N=1200rpm. SST turbulence model was used.

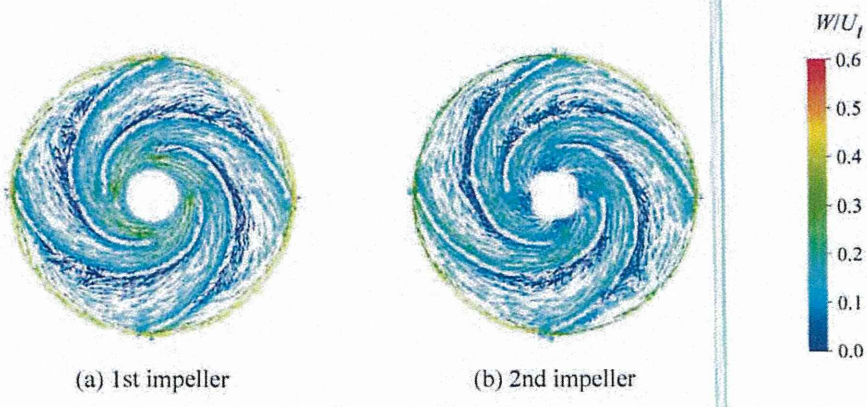

(a) 1st impeller (b) 2nd impeller

Fig. 12 Velocity vector near the back shroud of impellers with β_2=20deg in Prototype 2 at $Q=Q_d$ and N=1200rpm. SST turbulence model was used.

still improved, but better flow fields are achieved in Prototype 2, compared to the flow fields of Prototype 1.

5.5 Anti-Hemolysis and Thrombosis Performances at Off-Design Operating Conditions

The wall shear stress around the tongue at Q=1.63Q_d is shown in Fig.16. Q=1.63Q_d with the water at N=1150rpm corresponds to Q=5L/min with the blood at N=4000rpm. The region with the shear stress higher than 16Pa can be observed and it is thought to be caused by the increase of the flow velocity. The shear stresses on the walls except around the tongue were similar to those at Q=Q_d and the flows in the impellers and the return channel were smoother than those at Q=Q_d. The velocity vector near the back shroud of 1st impeller at Q=0.33Q_d is shown in Fig.17. Q=0.33Q_d with the water at N=1150rpm corresponds to Q=1L/min with the blood at N=4000rpm. The flow separation can be observed over a wide region of the pressure surface of the blades in Fig.17. As the flow velocities are small due to the low flow rate, the operations with the low flow rate have a possibility of the occurrence of the thrombosis in the stagnation caused by the flow separation. The flow separations were also observed in the 2nd impeller and the return channel. The wall shear stresses at Q=0.33Q_d were similar to those at Q=Q_d. Therefore, in the operations of Prototype 2, it is necessary to pay attention to the occurrence of the hemolysis at higher flow rates and the thrombosis at lower flow rates.

5.6 Pump Performance

The pump performance of Prototype 2 is shown in Fig.18. The horizontal axis shows the flow rate and the vertical axis shows the pump head. The experiment was conducted using the water at ordinary temperatures in the rotational speed of 1150rpm.

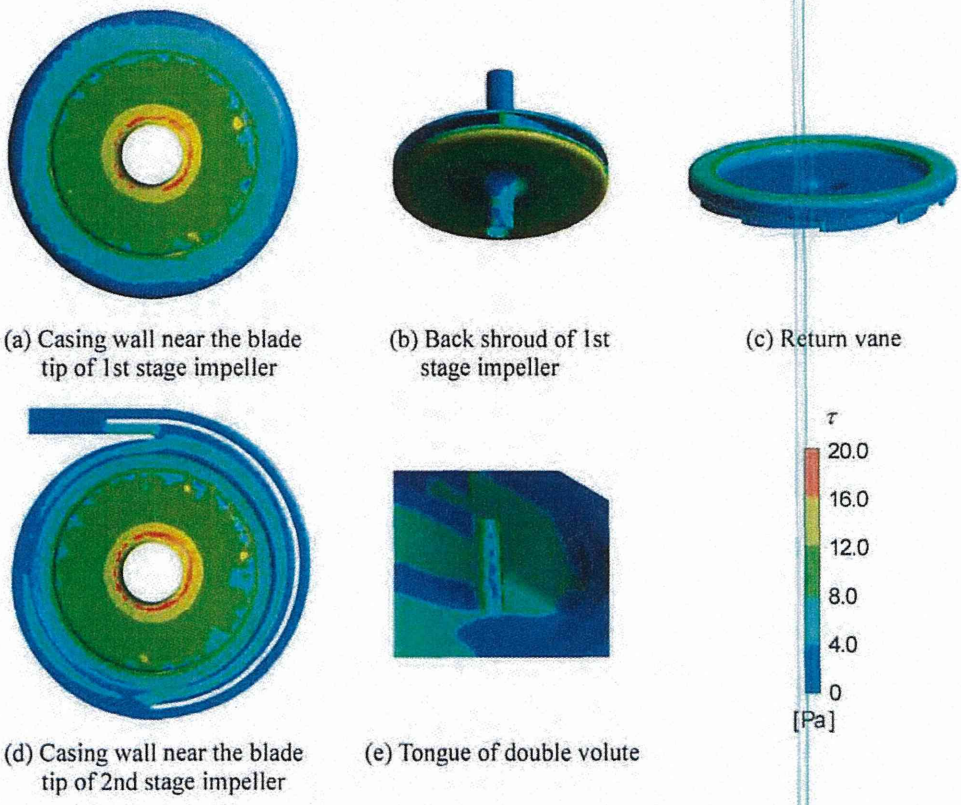

Fig. 13 Wall shear stress distribution on Prototype 2 at Q=Q_d. N=1150 rpm

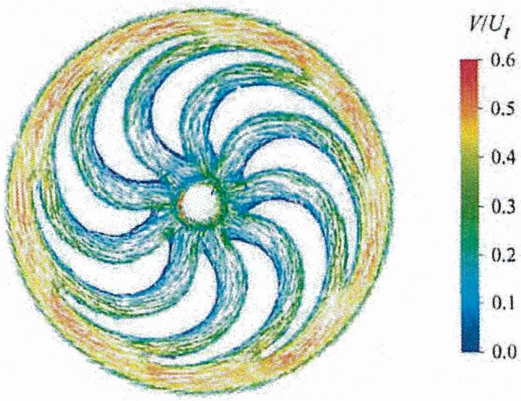

Fig. 14 Velocity vector on the cross-section (D'-D' in Fig.8) of the return channel in Prototype 2 at Q=Q_d. N=1150rpm

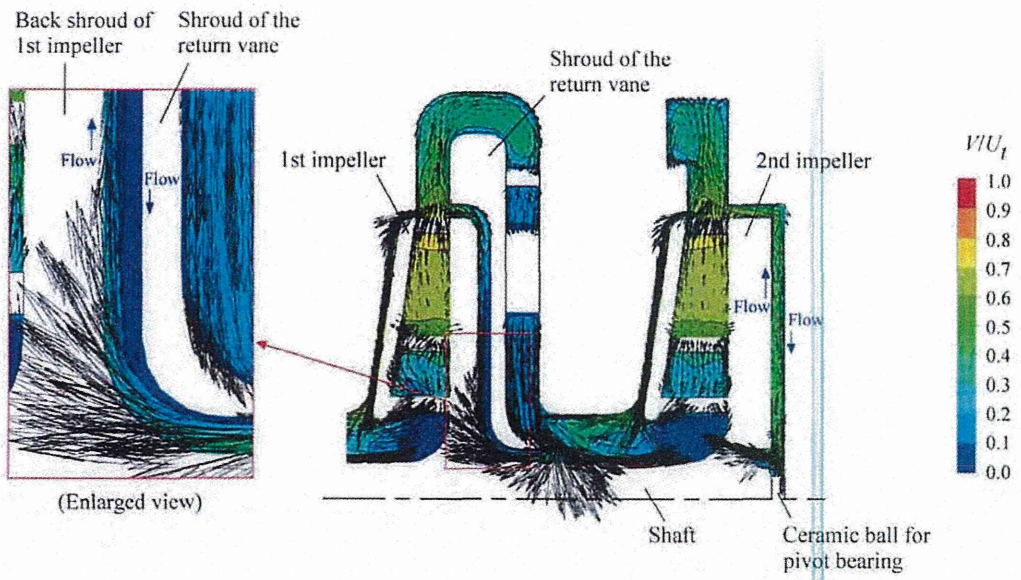

Fig. 15 Flow field on the meridian plane of Prototype 2 at $Q=Q_d$. N=1150rpm

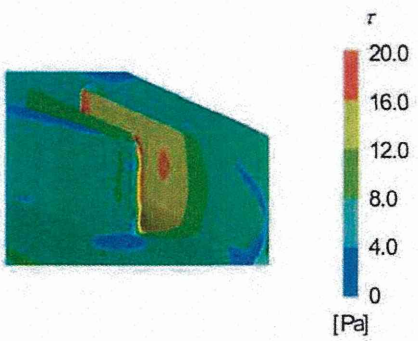

Fig. 16 Wall shear stress around the tongue of double volute of Prototype 2 at Q=1.63Q_d and N=1150rpm, which correspond to Q=5L/min and N=4000rpm with the blood

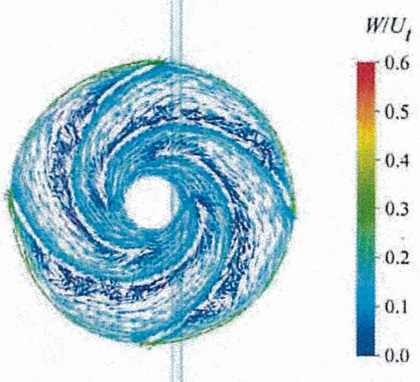

Fig. 17 Velocity vector near the back shroud of 1st impeller in Prototype 2 at Q=0.33Q_d and N=1150rpm, which correspond to Q=1L/min and N=4000rpm with the blood

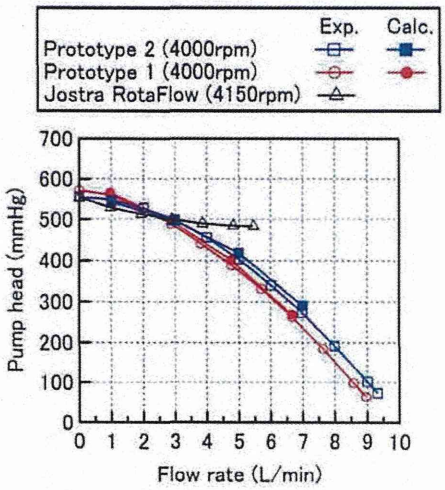

Fig. 18 Pump performance

Considering an easy understanding in clinical practice, the results were converted into the values in the operation with the blood at 4000 rpm, using the relation of $\Delta p_{blood} = \Delta p_{water} \cdot \rho_{blood} \cdot U_{t,blood}^2 / (\rho_{water} \cdot U_{t,water}^2)$. The pump performance of Prototype 1 is also plotted. The demanded pump performance of 500mmHg at 3L/min can be obtained and the performance curve is similar to that of Prototype 1. The pump performance of the Jostra RotaFlow centrifugal pump is also shown in Fig.18. The results was obtained through translating the results at 1200rpm with the water into the results at 4150rpm with the blood. The slope of the performance curve of Prototype 2 is steeper than that of the Jostra RotaFlow centrifugal pump in usable ranges of 1-5L/min, as in the case of Prototype 1. This indicates that the flow rate is insensitive to the flow resistance. This is an advantage because the stable flow rate can be kept easier. The computational results for Prototype 1 and 2 are shown in Fig.18. The computational results agree with the experimental results well.

The measurement of the efficiency except the torque due to the pivot bearings was conducted, but the stable values of the efficiency could not be obtained because the torque due to the friction in the pivot bearing was not stable in the operation with the air. This seems to be caused by the occurrence of the thrust load due to the decrease of the axial fluid force when the air is used as the working fluid. The efficiency which includes the friction loss of the pivot bearing was about 12% at $Q=Q_d$ and the maximum efficiency was about 15% at 5L/min.

5.7 Pressure Distribution

The pressure distributions in Prototype 1 and 2 are shown in Figs.19(a) and (b), respectively. The pressure was measured at the measuring points shown in Figs.5 and 9. In the case of Prototype 1, the flow rates were set to 0.29, 0.86, 1.44, 2.01, 2.57L/min at 1200rpm. These flow rates correspond to 1.0, 2.9, 4.8, 6.7, 8.6L/min at the operation of 4000rpm using the blood as the working fluid. In the case of Prototype 2, the flow rates were set to 0.29, 0.86, 1.44, 2.01L/min at 1150rpm. These flow rates correspond to 1.0, 3.0, 5.0, 7.0L/min at the operation of 4000rpm using the blood. In both cases, the results are converted into the values in the operation with the blood at 4000rpm. The horizontal axis represents the measuring point and the vertical axis represents the

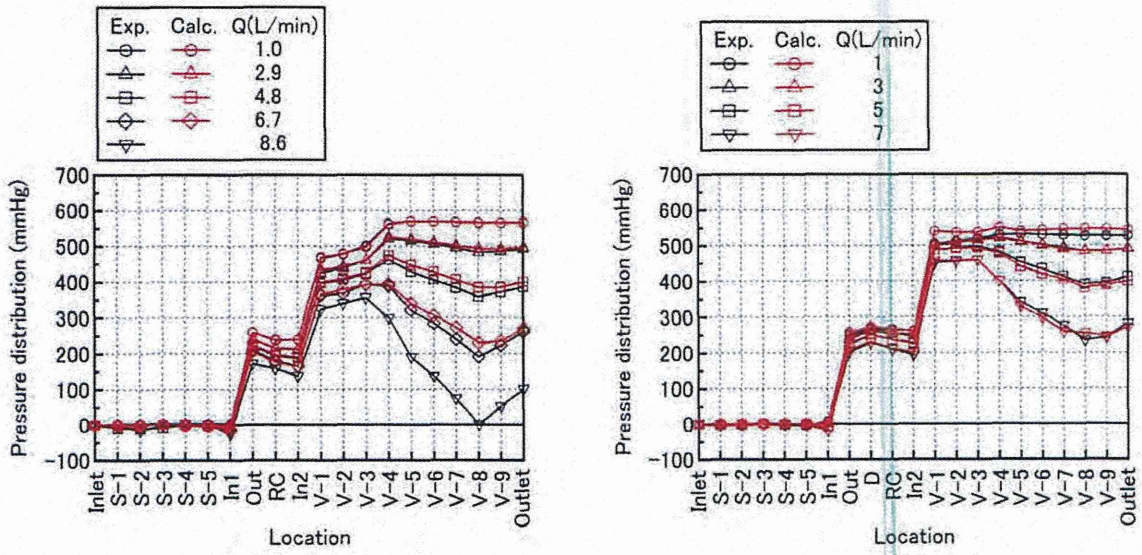

(a) Prototype 1 (b) Prototype 2

Fig. 19 Pressure distributions in the pumps

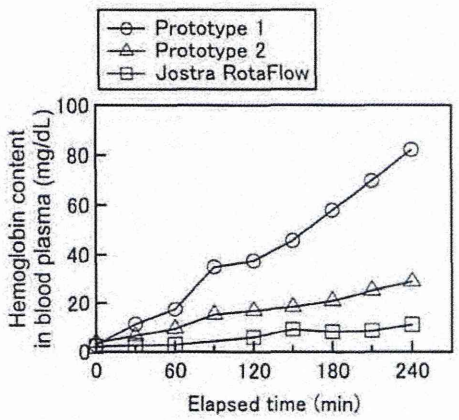

Fig. 20 Result of the hemolysis test with fresh goat blood at $Q=Q_d$ (3L/min) and $H=H_d$ (500mmHg)

difference of the pressure at the measuring point from the pressure at the inlet. The values at In1, Out, RC, In2 are the circumferentially averaged values. The experimental and computational results are shown by black and red colors, respectively.

The computational results are in good agreement with the experimental results. It was found that the work done by the 1st impeller (In1-Out) was almost the same as the work done by the 2nd impeller (In2-V-1) in both pumps of Prototype 1 and 2, as shown in Figs.19(a) and (b). It was also found that the pressure at the outlet (V-1) of the 2nd impeller in Prototype 2 was higher than that in Prototype 1 and the amount of the pressure recovery in the volute casing of Prototype 2 was not more than that in Prototype 1.

5.8 Hemolysis Test

The result of the hemolysis test is shown in Fig.20. The result is for the case that the flow rate and the pump head are the design values of 3L/min and 500mmHg, respectively. The horizontal axis represents the elapsed time and the vertical axis represents the hemoglobin content in the blood plasma. The rotational speeds of Prototype 1, 2, and the Jostra RotaFlow centrifugal pump were 4010rpm, 3980rpm, and 4240rpm, respectively. The amount of the hemolysis in Prototype 2 is as small as about one third of that in Prototype 1 after a lapse of four hours (240min). This shows that the design aimed at the decrease of the wall shear stress is effective for the decrease of the amount of the hemolysis.

As shown in Fig.20, the amounts of the hemolysis of Prototype 1 and 2 were larger than that of the Jostra RotaFlow centrifugal pump. In addition to further decrease of the wall shear stress, the design method considering the exposure time of the blood to a shear flow may be necessary because the exposure time is considered to affect the amount of the hemolysis [7, 8]. In the present study, it was also found that the hemolysis occurred at the high pump head of 500mmHg (at the high rotational speed) in the Jostra RotaFlow centrifugal pump, which is considered to have a high anti-hemolysis performance at lower pump heads (at lower rotational speeds). The realization of blood pumps with higher anti-hemolysis performance is desired.

5. Conclusions

The improvement of a prototype of two-stage centrifugal blood pump for the cardiopulmonary support system was conducted and the hemolysis test for the first prototype and the improved pump was performed. The results obtained in the present study are summarized as follows.

(1) Due to the attachment of the front shroud to the impeller, vortices which could cause the thrombosis occurred in the impeller. The occurrence of the vortices could be prevented by the change of the outlet blade angle of the impeller.
(2) The front shroud of the impeller was effective for the decrease of the wall shear stress on the casing near the tip of the impeller.
(3) The movement of the leading edge of the return guide vane and the tongue of the double volute casing away from the outlet of the impeller led to the decrease of the circumferential velocity around them and was effective to the decrease of the shear stress on them.
(4) The design method of the return guide vane which covered the region of the flow separation was effective for the suppression of the stagnation. The increase of the number of the vanes which led to the decrease of the region of the flow separation and the vane thickness was also effective for giving an uniform radial flow at the outlet of the return channel.
(5) The slope of the performance curve of the improved pump was as large as that of the first prototype. This is an advantage because the flow rate is insensitive to the change of the flow resistance. In the comparison of the pressure distributions, it was confirmed that the computational results agreed well with the experimental results.
(6) The amount of the hemolysis in the improved pump was about one third of that in the first prototype. This indicates that the decrease of the wall shear stress is effective for improving the anti-hemolysis performance of blood pumps.

Acknowledgments

The present study was supported by JSPS Grant-in-Aid for Scientific Research (B) (Grant Number 18360094 and 20360091 Principal Investigator: Dr. Tomonori Tsukiya).

Nomenclature

C	Tip clearance	Δp	Pressure difference
D_t	Diameter of impeller	μ	Viscosity
h	Blade height	ν	Kinetic viscosity
H	Pump head	ρ	Fluid density
N	Rotational speed	τ	Shear stress
Q	Volumetric flow rate	**Subscript**	
Re	Reynolds number ($=U_tD_t/\nu$)	1	Inlet
U_t	Tip speed of impeller	2	Outlet
V	Absolute velocity	*blood*	Blood
W	Relative velocity	d	Reference
β	Blade angle	*water*	Water

References

[1] Horiguchi, H, Tsukiya, T., Nomoto, T., Takemika, T., and Tsujimoto, Y., 2014, "Study on the Development of Two-Stage

Centrifugal Blood Pump for Cardiopulmonary Support System," International Journal of Fluid Machinery and Systems, Vol. 7, No. 4, pp.142-150. (DOI: 10.5293/IJFMS.2014.7.4.142)
[2] ANSYS, Inc., 2006, "Modeling Flow Near the Wall", ANSYS CFX-Solver Modeling Guide, Release 11, pp.125-127.
[3] ANSYS, Inc., 2006, "Modeling Flow Near the Wall", ANSYS CFX-Solver Theory Guide, Release 11, pp.110-111.
[4] Takeda, H., 2005, "Basic Design on Pumps (in Japanese)," Dengyosha Technical Review, Vol. 29, No. 2, pp. 7-14. (http://www.dmw.co.jp/technical/pdf/no57.pdf)
[5] Kameneva, M. V., Burgreen, G. W., Kono, K., Repko, B., Antaki, J. F., and Umezu, M., 2004, "Effects of Turbulent Stresses upon Mechanical Hemolysis: Experimental and Computational Analysis," ASAIO Journal, Vol. 50, No. 5, pp. 418-423.
[6] Stepanoff, A. J., 1957, "Centrifugal and Axial Flow Pumps (Second Edition)," John Wiley & Sons Inc., pp. 172.
[7] Heuser, G., Opitz, R., 1980, "A Couette Viscometer for Short Time Shearing of Blood," Biorheology, Vol. 17, pp. 17-24.
[8] Giersiepen, M., Wurzinger, L. J., Opitz, R., and Reul, H., 1990, "Estimation of Shear Stress-Related Blood Damage in Heart Valve Prostheses – in Vitro Comparison of 25 Aortic Valves," The International Journal of Artificial Organs, Vol. 13, No. 5, pp. 300-306.